AMB2022-02 Benchmark Measurements and Challenge Problems

Modelers are invited to submit simulation results for any number of challenges they like before the deadline of 23:59 (ET) on July 15, 2022. Tabulated results using the challenge-specific templates are required for most challenge problems and simulation results may be submitted **here**. An informational webinar for AMB2022-01 and AMB2022-02 will be held on May 5, 2022, from 10:30 – 12:15 Eastern Time. The webinar registration link is **here**. After the webinar is completed, links to the recorded presentations and to a FAQ page will be added to the AMB2022-02 description page. Additional information may become available later so updated versions of this document may be posted. Please check back occasionally.

All evaluations of submitted modeling results will be conducted by the AM-Bench 2022 organizing committee. Award plaques will be awarded at the discretion of the organizing committee. Because some participants may not be able to share proprietary details of the modeling approaches used, we are not requiring such details. However, whenever possible we strongly encourage participants to include with their submissions a .pdf document describing the modeling approaches, physical parameters, and assumptions used for the submitted simulations.

Please note that the challenge problems reflect only a small part of the validation measurement data provided by AM Bench for each set of benchmarks. The Measurement Description section, below, describes the full range of measurements conducted.

AMB2022-02: Laser powder bed fusion (LPBF) 3D builds of nickel-based superalloy IN718 test objects incorporating ***three different custom laser scan strategies***. Detailed descriptions are found below, and simulation results may be submitted **here**.

Challenges

- Time Above Melting Temperature (CHAL-AMB2022-02-TAM): Time above the midpoint between the solidus and liquidous temperatures for the melt pool at specified locations within the build volume. This metric is closely related to melt pool length but is explicitly location specific.
- Solid Cooling Rate (CHAL-AMB2022-02-SCR): Cooling rate immediately following complete solidification (below solidus) at specified locations within the build.
- Part Deflection (CHAL-AMB2022-02-PD): Deflection of the as-built (no heat treatment) bridge structure after it is partially separated from the build plate.

Please note that all of the Part Deflection measurement results for the CHAL-AMB2022-02-PD may not be available at the time model result submissions are due so the data release and submission judging may be delayed. Modelers should periodically refer back to this document for updates.

5. Data to be Provided
6. Relevant References

---

1. Overview and Basic Objectives

The AMB2022-02 benchmarks use laser powder bed fusion (LPBF) 3D metal alloy builds of a bridge structure geometry that has 12 legs of varying size, as shown in Figure 1. All of the legs are solid except for leg 10 that is hollow with thin internal walls.

The modeling challenges fall into two categories: in-situ thermographic measurements, and ex-situ deflection measurements. The in-situ thermographic measurements involve the same challenges as the AMB2022-01: the local ***cooling rates*** immediately after solidification, and the ***time above melting*** temperature. The ***distortion*** of the part after partial cutting from the base plate will also be conducted similarly to AMB2022-01. *Partial submissions to individual challenges will also be accepted.*

Many of the pertinent data for these challenges, including precursor material characterization and part CAD files, can be found in the AMB2022-01 challenge dataset **here**. The custom scan strategy data for AMB2022-02, which are unique from AMB2022-01, are found in a separate dataset **here.**

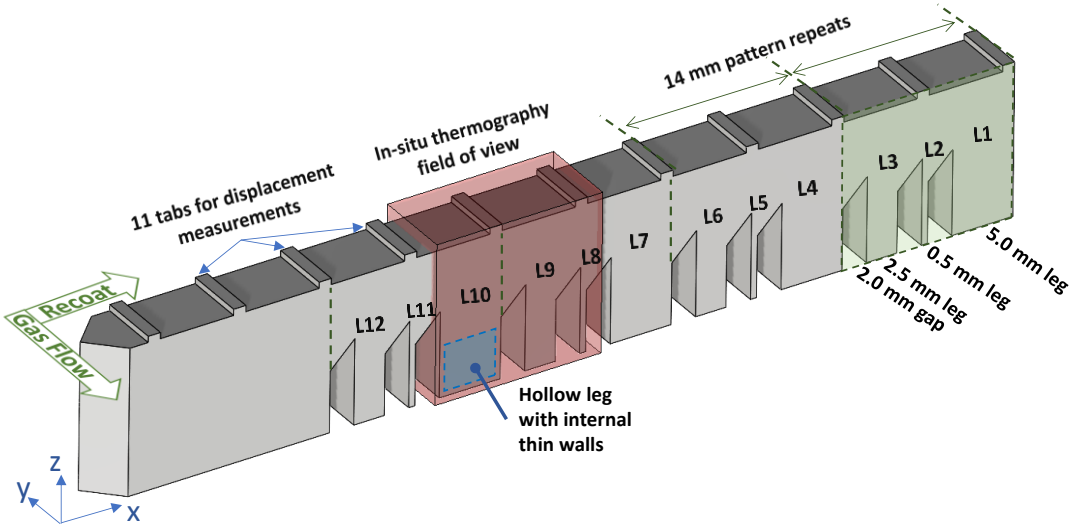

Figure 1: Overview of the AMB2022-01 and -02 bridge structure geometry with labelled legs (e.g., L1 to L12), hollow Leg 10, and region where in-situ thermography is applied.

2. Build and Post-Build Processing Description

2.1 Materials and Part Design

2.1.1 Substrates:

Nickel alloy IN718 AM parts are built on substrates (build plates) consisting of nominally the same alloy. The substrates are 100 mm squares, 12.5 mm thick, and mounted from below using four ¼-20 cap screws in direct contact with a custom 304 stainless steel baseplate. Substrates for the AMB2022-02 measurements did not include in-situ thermocouples, although modelers may wish to consider results from the AMB2022-01 builds.

2.1.2 Part layout on the build plate:

Four bridge-structure parts (labeled P1 to P4) and two recoater guides (labelled G1 and G2) are fabricated on each build plate, as shown in Figure 2. Each bridge part is identical. They are spaced by 20.5 mm along the Y-axis, and they are offset from each other along the X-axis by 2.0 mm so that the recoater blade progressively engages each one. The guides G1 and G2 are solid structures used to ensure the recoater does not damage the bridge structures. The recoating direction and laminar gas flow direction are also shown. Stereolithography (STL) and STEP files which includes CAD geometry of the build plate, parts, and their relative locations can be found in the /CAD_Geometry/ directory of the AMB2022-01 challenge description dataset, which utilizes the same part geometry as AMB2022-02. Note that users should refer to the AMMT scan strategy description and data in Section 2.3 which are specific to the AMB2022-02 challenges.

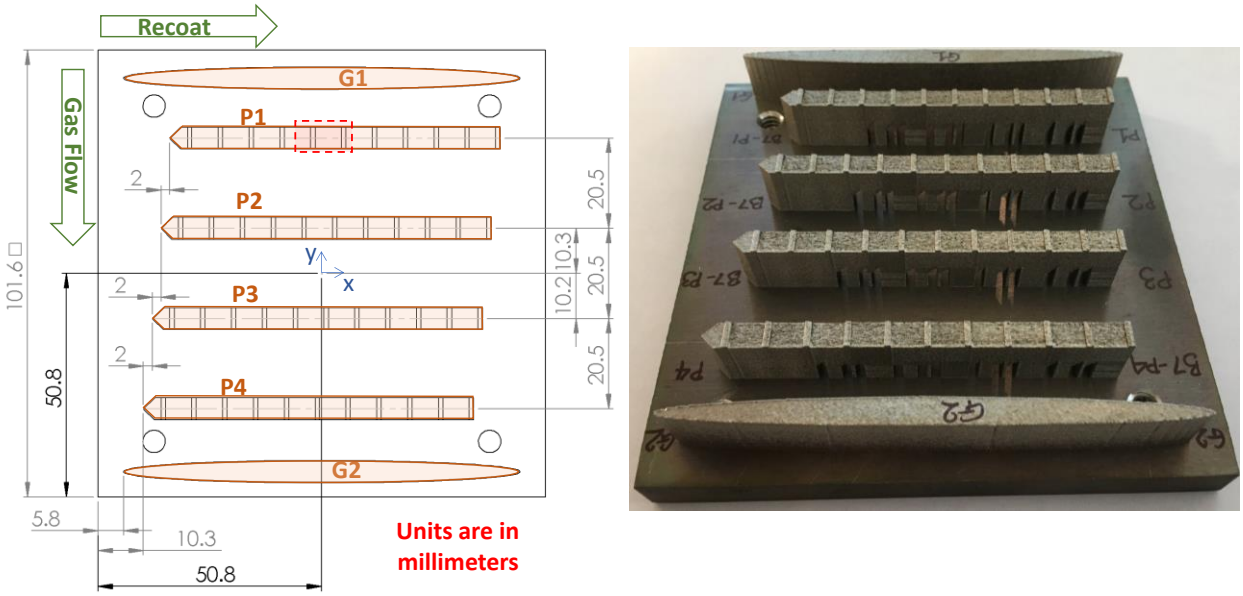

Figure 2: Left: Geometric layout of the four bridge structure parts (P1 to P4), two recoater guides (G1 & G2) and AMMT coordinate center on the build substrate. Right: Photograph of Build #7 (B7) from the AMB2022-01 builds with labelled parts.

2.1.3 Individual part geometry:

Figure 3 presents a schematic of the bridge structure part that is 75 mm long, 12 mm tall, and 5 mm wide with 7 mm tall 'legs' that form into 45° overhangs below a solid structure. The recoating direction starts at the pointed end with the 45° taper, and proceeds left. CAD geometry of the entire build with 6 parts, or individual bridge-structure or recoater guide structures are available as STEP or STL geometry files in the \CAD_Geometry\ directory of the AMB2022-01 challenge description dataset, which utilizes the same part geometry as AMB2022-02.

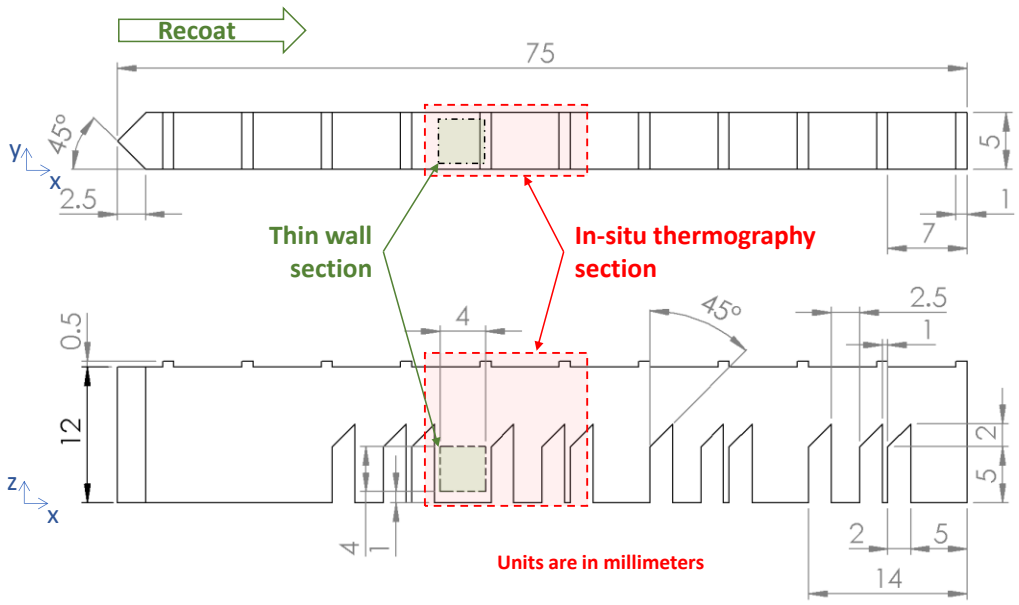

Figure 3: Plan (top) and elevation (bottom) views of the AMB2022-01 and -02 bridge structure external geometry. Part 1 (P1) is the only part to include in-situ thermography used in AM-Bench challenges.

Leg L10 of each as-built part has a hollow cavity with four thin-wall structures shown in Figure 4. The outer walls of the L10 leg are approximately 0.5 mm thick and enclose two thin walls that are the width of a single laser track and another two that are the width of a double laser track. The thin walls are aligned parallel to the recoater blade direction. The bottoms of the walls sit on a solid base that is 1 mm thick, and the walls are built 4 mm high before a flat-bottomed ceiling is built. The inner regions of the L10 legs are completely sealed once the parts are built so the resulting gas and powder filled pockets preclude heat treatments until EDM cutting of the parts is completed.

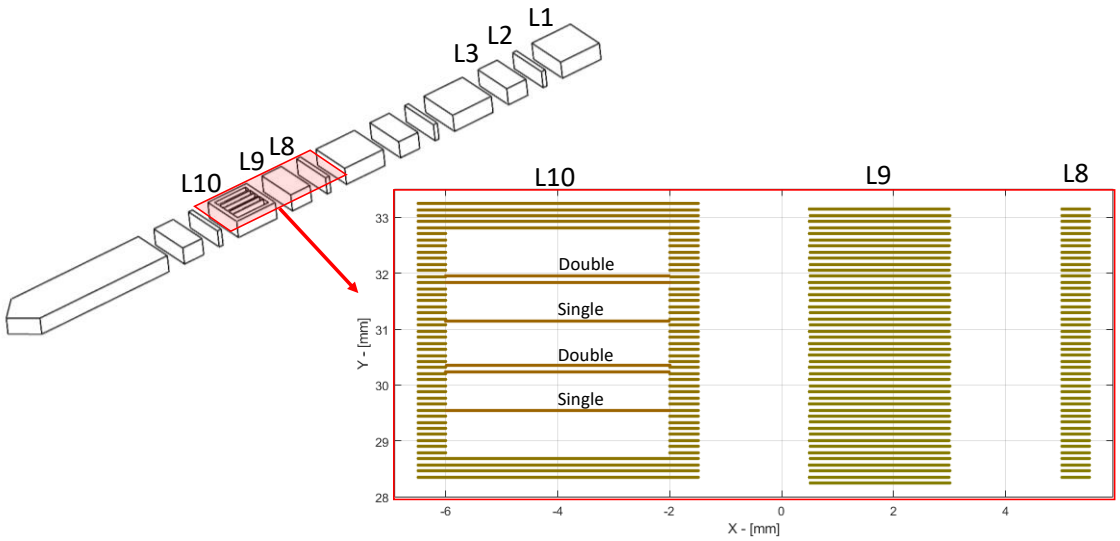

Figure 4: Leg numbering and expanded view of the scan strategy (Layer 50) for the AMB2022-01 builds that constructs the thin-wall structures within Leg 10 (L10). AMB2022-02 builds have the same thin wall structures. Refer to Section 2.3 on scan strategy for more precise description.

2.1.4 Feedstock Material:

All IN718 builds were conducted using powder from a single lot and the particle size distribution (PSD), nominal powder density, and chemical composition are provided in Table 1. The powders were kept sealed in the original shipment containers until use. Virgin powder was used for each build.

Powder PSD was also measured by NIST. Samples were acquired utilizing methods outlined Sec. 7.1.2 of ASTM B215-15. PSD was measured using a commercial dynamic imaging analysis (DIA) system, with measurement method described in ISO 13322-2:2006. Details on NIST DIA-based PSD measurement method and uncertainty analysis are available in Whiting et al. 2019. A Mill Test Certification supplied by the manufacturer for the IN718 power, and NIST PSD measurement results data are available in the /Materials directory in the AMB2022-01 challenge description dataset, which utilized the same powder lot as AMB2022-02.

Table 1: Precursor material information.

Particle size distribution (PSD) - Vendor-supplied values are taken from vendor-supplied data sheets, which utilized sieve analysis following ASTM B214. - NIST-measurement based on commercial DIA system, and based on Xc_min metric.	Vendor: D_{10} = 17.53 µm D_{50} = 31.98 µm D_{90} = 53.79 µm	NIST: D_{10} = 16 µm D_{50} = 27 µm D_{90} = 46 µm
Powder density - The value in this table was taken from vendor-supplied data sheets, which followed ASTM B417	4.05 g/cm^3	
Chemical Composition - Values in this table are taken from vendor-supplied data sheets, which utilized ASTM E1479 (inductively-coupled plasma atomic emission spectrometers) for all elements except for using ASTM E1019 (combustion) for C/S, ASTM E1019 (fusion) for O/N/H, and ASTM E1184 for Bi/Pd/Se/Ag. - All composition measurements are in mass (weight) percent.	Fe = Balance Ni = 53.48 Cr = 18.40 Nb = 5.48 Mo = 3.01 Ti = 1.00 Al = 0.48 Co = 0.02 Cu < 0.01 Si = 0.03 Mn < 0.01 Ta < 0.01 C = 0.05 S < 0.005 P < 0.01 B = 0.003 Ag < 0.0001 Pd < 0.0001 Se < 0.0001 Bi < 0.00003 O = 0.014 N = 0.011 H = 0.0006	

2.2 Build Parameters, Scan Strategy, and Build Conditions

Three builds with custom scan strategies were conducted using the NIST Additive Manufacturing Metrology Testbed (AMMT) which is a NIST-designed and built laser-processing metrology platform. Detailed references to the AMMT design, controller, and various other research may be found here. The AMMT is also a fully functional laser powder bed fusion (LPBF) AM machine, with a continuous-wave (CW) ytterbium fiber (Yb:fiber) laser, with a central wavelength of 1070 nm, directed by fully-controllable scanning galvanometer mirrors. The controlled laser scanning is synchronized to various measurement instrument triggering and data acquisition.

2.2.1 Nominal build parameters:

Table 2 outlines the different scan strategies for the three AMB2022-02 3D builds, and the corresponding scan strategy data file names for each. Table 3 gives the nominal processing parameters and conditions used during the AMB2022-02 3D builds. Note that the laser spot size for the 'nominal' conditions is D4σ = 77 µm.

Table 2: Scan strategy descriptions for the three parts V6, V7, and V8 constructed as part of AMB2022-02

Build #	Scan Strategy Data Filename	Scan strategy description
V6	AMB2022-02-AMMT-XYPT-V6.h5	Constant laser power, alternate scan stacking
V7	AMB2022-02-AMMT-XYPT-V7.h5	'Interleaved' scans with alternating laser power of 171 W and 285 W between tracks.
V8	AMB2022-02-AMMT-XYPT-V8.h5	Pre-sintering (diagonal scans) at 85.5 W and 230 µm spot size, followed by standard 285 W.

Table 3: Nominal build conditions for the AMB2022-02 bridge-structure parts.

AMMT Nominal Commanded Build Conditions	
Laser power	V6: constant 285 W V7: 171 W and 285 W V8: 85.5 W pre-sinter then 285 W
Laser speed	960 mm/s
Hatch spacing	110 µm (V8 pre-sinters at 220 µm)
Layer thickness	40 µm
Laser energy distribution	Rotationally-symmetric Gaussian
Laser spot size	77 µm D4σ (V8-P1-P4 pre-sinters at 170 µm, V8-P2-P3 pre-sinters at 380 µm
Total number of layers	312
Inert gas	Argon
Max. Oxygen level	< 1 000 ppm
Gas flow speed (@ Z = 10 mm)	4.3 m/s
Gas flow direction	-Y
Chamber pressure	95 ± 5 kPa

2.3 Scan Strategies

Figure 5 details the general order in which each part is scanned by the laser. Note the color bar on the left of the image, which indicates the order of laser scan via colormap. This general part-to-part order repeats for all layers.

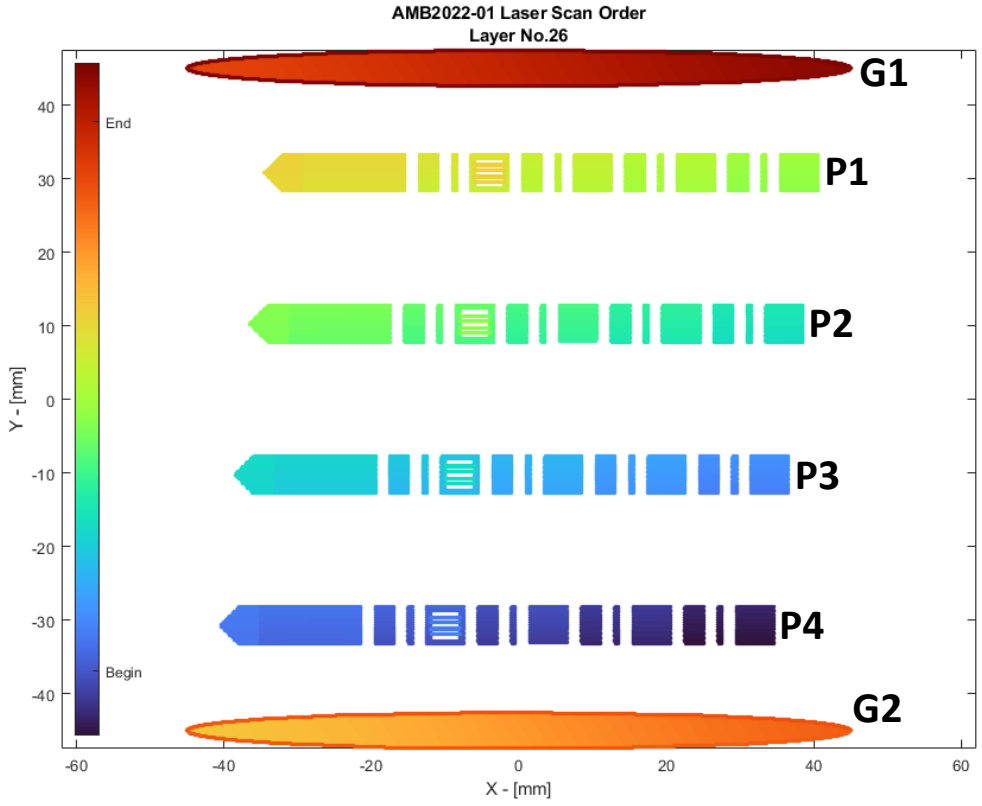

Figure 5: Example scan order in which each layer scans proceeds as follows: P4, P3, P2, P1, G2, G1. The order in which individual parts are built is the same for all layers.

The general order and progression which the laser scans each part is nominally similar to those described in AMB2022-01. Users should refer to that document for general outline of general sequence or order in which parts are scanned by the laser. However, each of the three AMB2022-02 builds utilize 'alternate scan stacking', shown in Figure 6. In contrast to the strategy used in AMB2022-01, this strategy alternates the specific location of each scan track for subsequent layers, so tracks on upper layers do not directly overlap with those below.

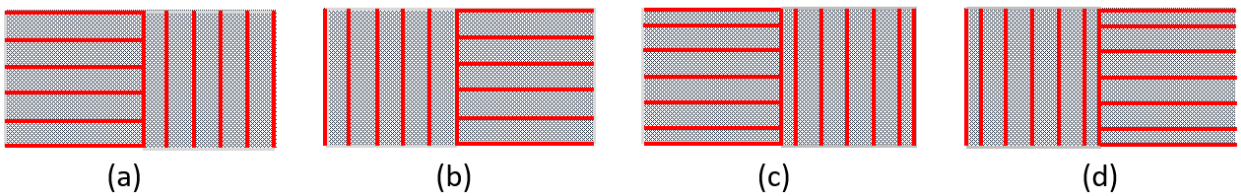

Figure 6: Alternate scan stacking strategy for builds V6, V7, and V8, which proceed a,b,c,d. AMB2022-01 builds proceed a,b,a,b (no stacking).

2.3.1 V6: Standard Parameters with Alternate Scan Stacking

Build V6 utilized the same nominal laser power, spot size, scan speed, and scan strategy sequence as the 3D builds described in AMB2022-01. However, these utilize the alternate scan stacking described above and in Figure 6.

2.3.2 V7: Interleaved Scans with Alternating Laser Power

Build V7 utilized 'interleaved' scans, in which every even track is first formed at a lower laser power of 171 W, followed by each odd track formed at the higher nominal power of 285 W. Figure 7 demonstrates this sequence, with each sub-figure described as follows:

a) Initial 171 W scan of even tracks in first region
b) 285 W scan of odd tracks in first region
c) 171 W scan of even tracks in second region
d) 285 W scan of odd tracks in second region.
e) 285 W scan of odd tracks in fourth region, which includes hollow leg 10.
f) 285 W thin horizontal walls made in leg 10.

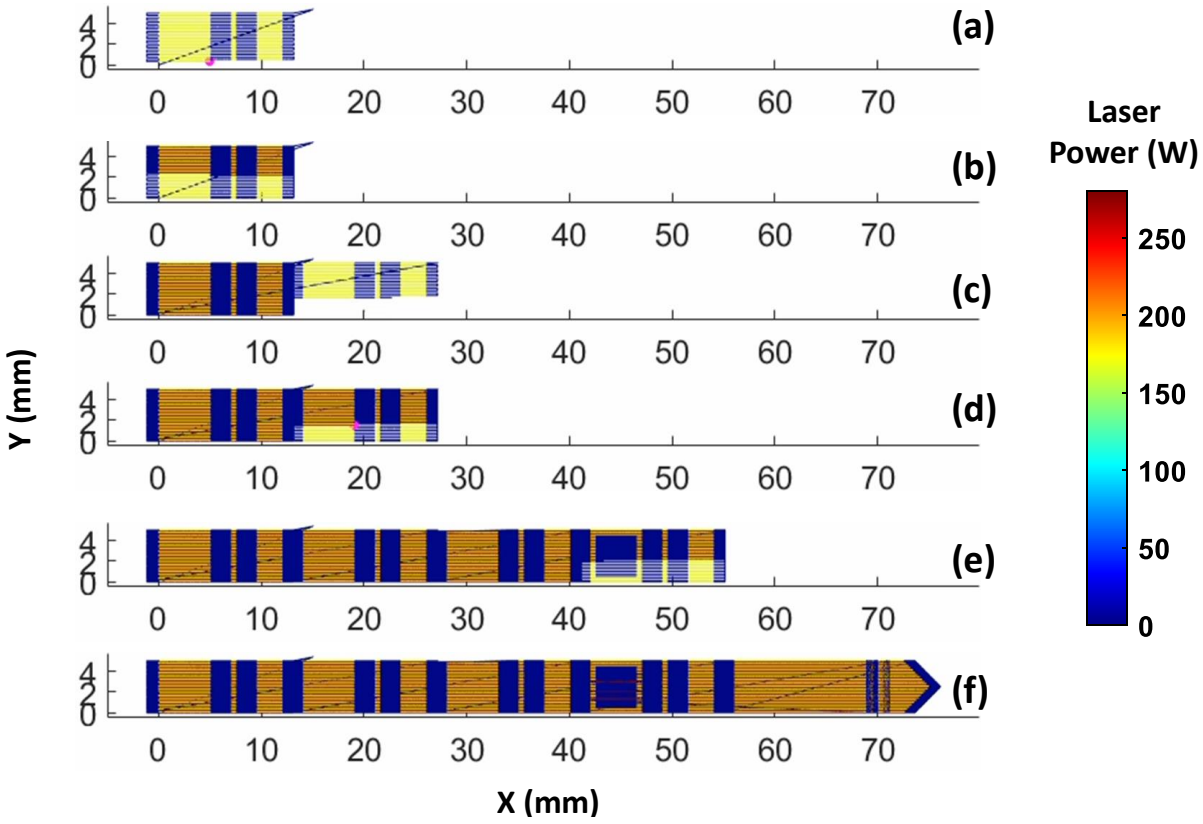

Figure 7: Scan sequence for V7 parts, with laser power plotted in color. Note that laser 'off' is in dark blue, and part orientation is reversed in X in the plots with respect to the standard AMMT machine coordinates in Figure 5.

2.3.3 V8: Presintering Scans

Build V8 utilized a 'pre-sintering' scanning strategy shown in Figure 8 and Figure 9. This sequence first scans the entire part in a diagonal direction with a 0.3x lower laser power (85.5 W), larger laser spot size (D4σ = 170 µm fo parts 1 and 4, and D4σ = 380 µm for parts 2 and 3), and 2x wider hatch spacing (220 µm) than the nominal laser parameters (D4σ = 77 µm). This pre-sintering is then followed by the standard laser scan parameters used in the V7 part, which includes the alternate scan stacking described in Figure 6. The following steps describe the pre-sintering sequence for one of the example bridge structure parts shown in Figure 8.

a) Pre-sinter region 1 (85.5 W laser power, D4σ = 310 µm laser spot size, 220 µm hatch spacing)
b) Pre-sinter region 2
c) Pre-sinter final section
d) Standard laser scan parameters on region 1 (285 W laser power, D4σ = 77 µm laser spot size, 110 µm hatch spacing
e) Final section using standard laser scan parameters

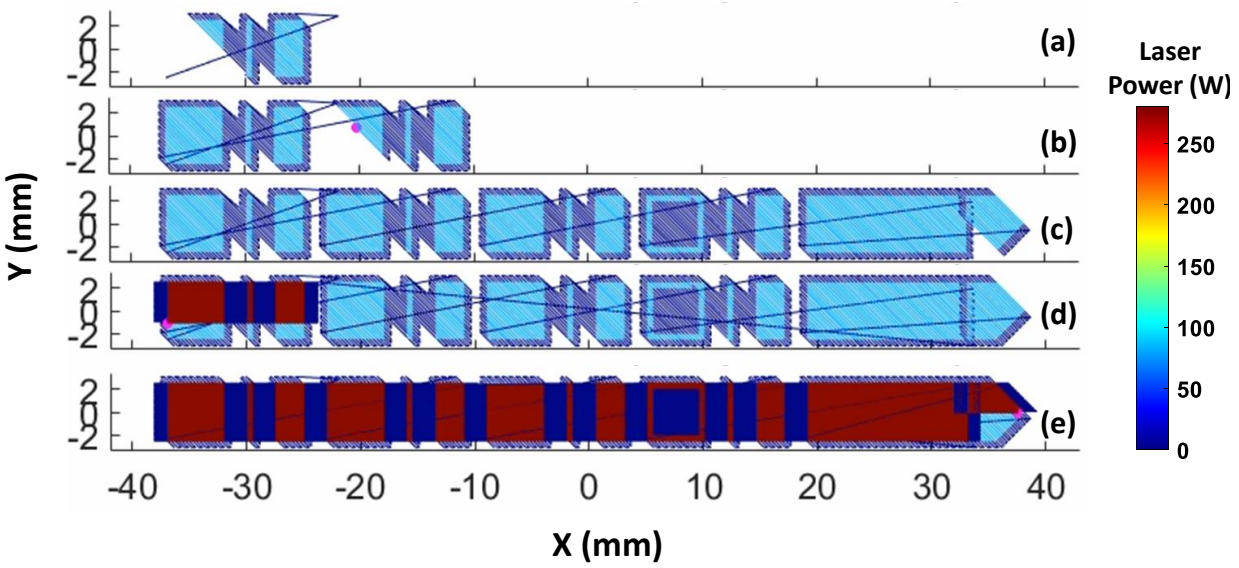

Figure 8: Scan sequence for V8 parts, with laser power plotted in color. Note that laser 'off' is in dark blue, and part orientation is reversed in X in the plots with respect to the standard AMMT machine coordinates in Figure 5.

Parts 1 and 4 have a smaller pre-sintering spot size (170 µm) compared to parts 2 and 3 (380 µm), as shown in Figure 9. Note that the modeling challenges based on in-situ thermography are only applied to Part 1 (P1).

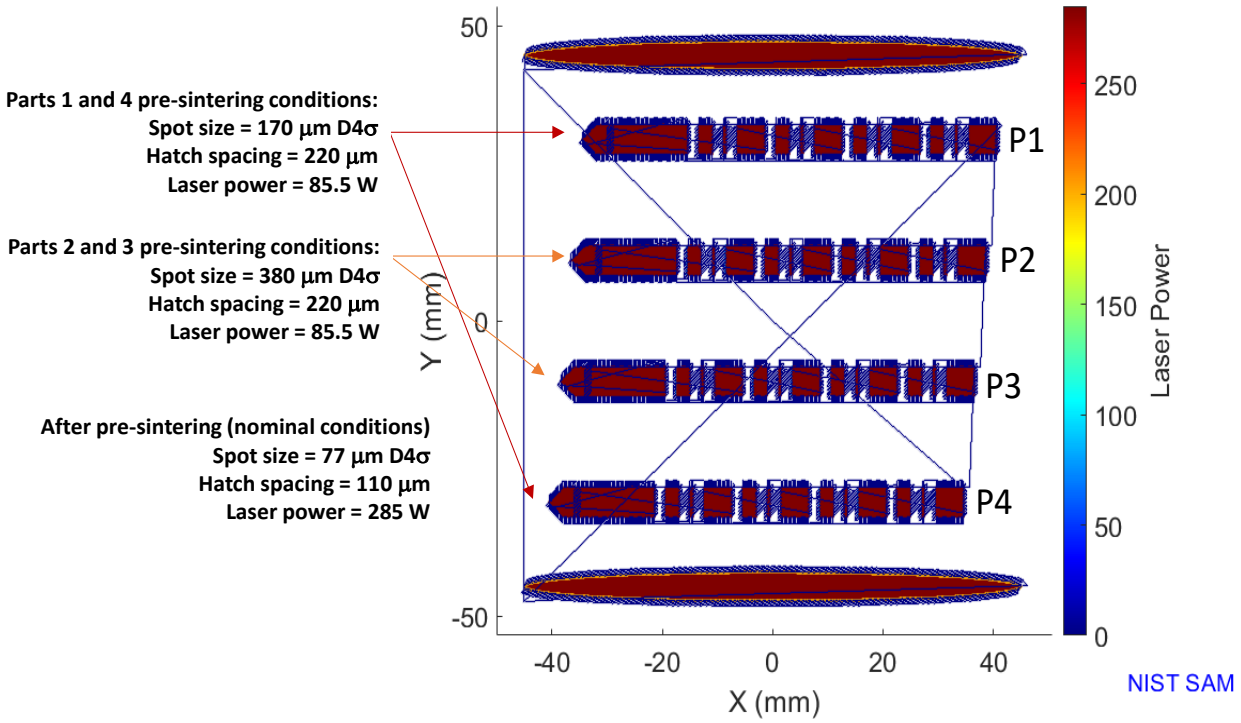

Figure 9: Different pre-sintering conditions for each part in the V8 3D builds.

2.3.4 Detailed Scan Strategy Data:

While the nominal build parameters and general laser scan strategy are described above, these do not fully define the order, timing, or position the laser scans throughout the build. The AMMT is a completely open build platform allowing us to provide unambiguous scan strategy data. The complete scan strategy for each of the AMB2022-02 custom 3D builds are available as single HDF5 files in the AMB2022-02 Challenge Description Dataset, and listed in Table 2.

The HDF5 file's /XYPT/ subgroup contain 312 numbered subgroups representing each layer's scan strategy data (e.g., /XYPT/1/ for layer 1). Each layer subgroup then contains five vectors: X, Y, P, T, and D corresponding to the digital commands executed by the AMMT. These represent the laser spot X-position in [mm], Y-position in [mm], commanded laser power in [W], and an instrument trigger (an unsigned integer), and the commanded spot size in [mm].

The corresponding time period between each element within the X, Y, P, T, and D vectors correspond to 10 µs, or a digital command rate of 100 kHz. Note that these are the *commanded* positions sent to the AMMT controller, whereas the *actual* traversed scan position and timing may be affected by laser or galvo calibration errors (Lane et al. 2020, Yeung et al. 2020), dynamic galvo positioning error (Yeung et al. 2016), or dynamics of the laser on/off modulation (Grantham et al. 2016), though these should be minimal for most modeling purposes.

Additionally, example Matlab scripts for extracting data and creating the above plotting the HDF5-based scan strategy are available in the /Scan_Strategy/ directory of the AMB2022-01 challenge description dataset.

2.3.5 Gas flow system:

Inert gas flow across the laser melting process is used to remove process byproducts (metal vapor, condensate, and ejecta) from the laser path, build area, and chamber windows. Previous studies have shown that ineffective gas flow interferes with laser delivery and may result in powder bed contamination (Ladewig et al. 2016, Deisenroth et al. 2021). The AMMT gas flow system incorporates a two inlet and one outlet system, as shown in Figure 10a. As shown by the orientation of the fabric tufts in Figure 10a, the inlet locations at the top and bottom of the process enclosure prevent the formation of a recirculation zone that would reduce the efficacy of byproduct transfer to the outlet.

The total flow rate of argon through the build chamber was approximately 390 L/min. This flow rate and nozzle configuration results in spatial distributions of the gas flow speed in the Y and Z directions, which are approximately invariant in the X direction across the build area. The combined speed resulting from the Y and Z velocity components of the flow was measured by hot wire anemometry at several Y and Z locations at approximately X = 0 mm to characterize the flow across the build space. Details of the speed measurement are described in Weaver et al. 2021. As shown in Figure 10b, the gas speed at the single track and pad location (near X = 0 mm, Y = 30 mm) at Z = 10 mm is approximately 4.3 m/s, which is used as a representative gas flow speed value.

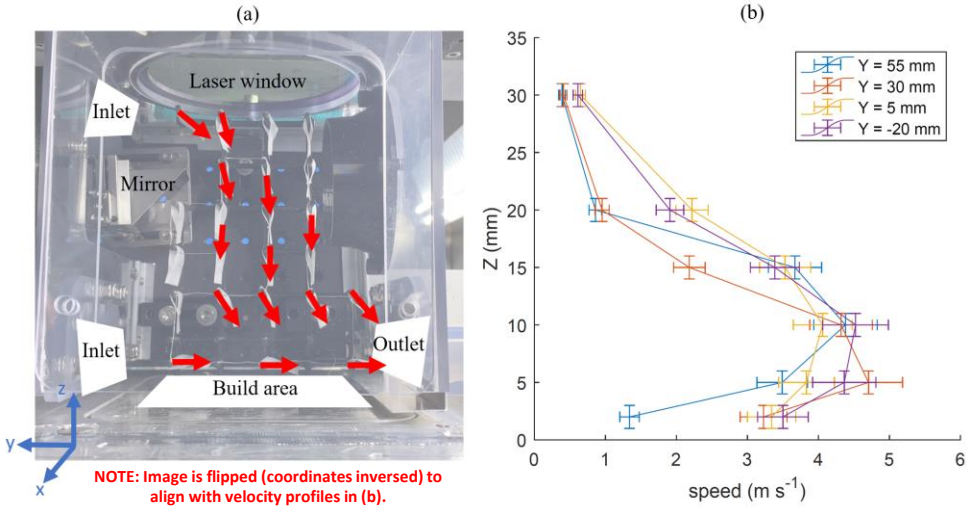

Figure 10: (a) AMMT process enclosure gas flow direction distribution based on fabric tufts. The image is flipped horizontally for ease of visualization and approximate axis directions (not origin) are shown. (b) gas flow speed distributions at varying Y and Z positions at approximately X = 0 mm.

2.4 In Situ Monitoring Systems

Figure 11 a) shows a diagram of the staring imaging system used for in situ thermographic measurements and b) shows a photograph of the completed system. To the greatest extent possible, this system was designed to provide nearly identical layer scan patterns, measurement methods, instruments, and gas flow conditions for the sets of 3D build benchmarks (AMB2022-01 and AMB2022-02) and the 2D bare plate benchmarks (AMB2022-03).

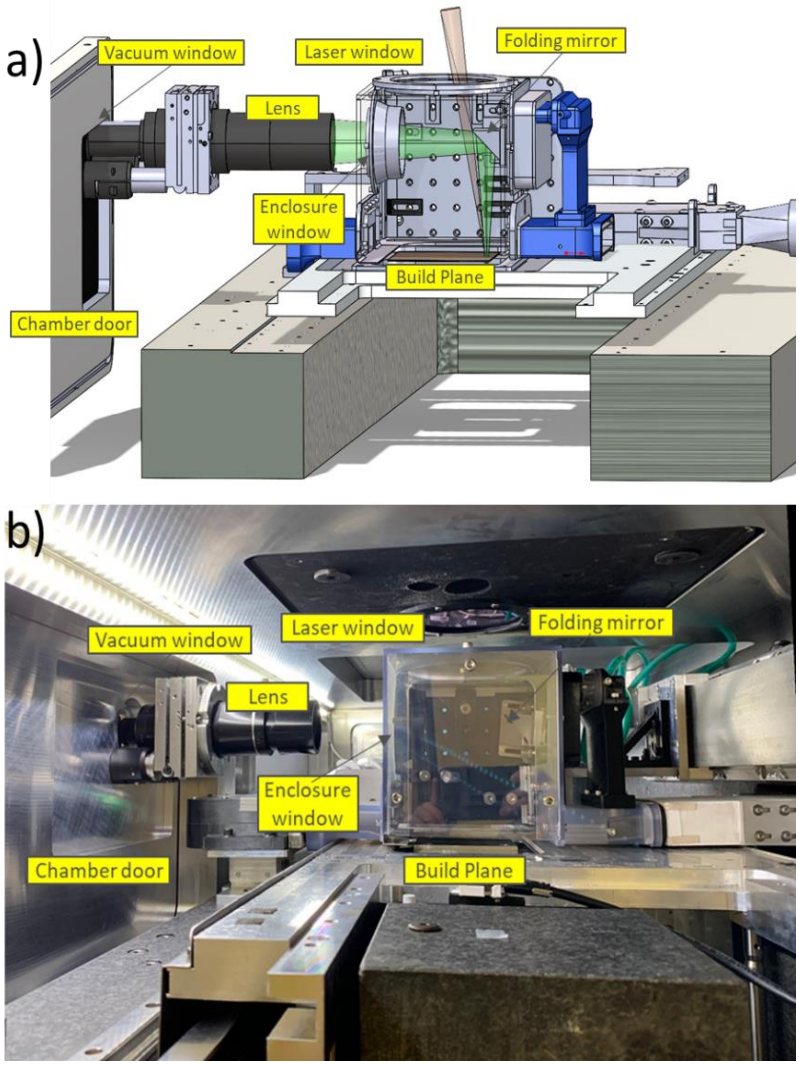

Figure 11: Staring thermal imaging system used for in situ thermography on the AMMT, a) CAD model and b) photograph.

The properties of the camera used for the in situ thermography measurements are given in Table 4. Although this camera is capable of frame rates greater than 30 kHz, practical considerations limited us to 8.333 kHz for the 3D builds., which is still far better than the 1.8 kHz that was possible for AM Bench 2018. This high data rate makes it impossible to take data continuously throughout the build within the region of interest, so data were acquired using the layer scheme: 1, 2, 5, 6, 9, 10… This scheme allows direct comparison between adjacent odd-even build layers. These data have been converted into a complete spatial 3D data set by copying from nearby layers with the same laser path direction. This layer measurement scheme includes redundancy compared with the more sparse 1, 4, 7, 11… data collection scheme.

Table 4: Camera properties for high-speed staring thermography camera in the AMMT

Sensor Type:	Si-based CMOS
View Angle:	~90°
Wavelengths:	830 nm to 870 nm
Magnification	1x
Window Size (x by y):	(640 by 304) pixels
iFoV (x by y)	(20.4 by 20.8) µm/pixel
FoV (x by y)	13.4 x 6.4 mm
Frame Rate	8333 frames/s
Integration Time	20 µs
Bit depth:	12-bit (4096 DL)
Calibrated Temperature Range:	1001 °C to 1389 °C

The field of view (FoV) for the in-situ thermography is marked by the red box in Figure 1. It encompasses the entirety of Legs 8, 9 and 10. The FOV is offset from the island section geometry so that the thermography captured from the small and medium legs are indicative of the nominal thermal history of the other small/medium legs.

2.5 Sample Cutting

Before conducting ex situ measurements, the 4 parts on each build plate are separated from one another via EDM cutting, as shown in Figure 12. As a result, the parts used for distortion and residual strain measurements are attached to a smaller portion of build plate material than during the build. The remaining build plate material measures 100 mm ± 1 mm long, 11 mm ± 1 mm wide, and 12.5 mm thick. This is the state of the samples when measuring residual strains using synchrotron X-ray diffraction as well as the starting condition when measuring part deflection. Smaller samples used for microstructure and XRCT studies were also extracted using EDM. Currently, only part deflection measurements are scheduled but future measurements of residual strains and microstructure are planned.

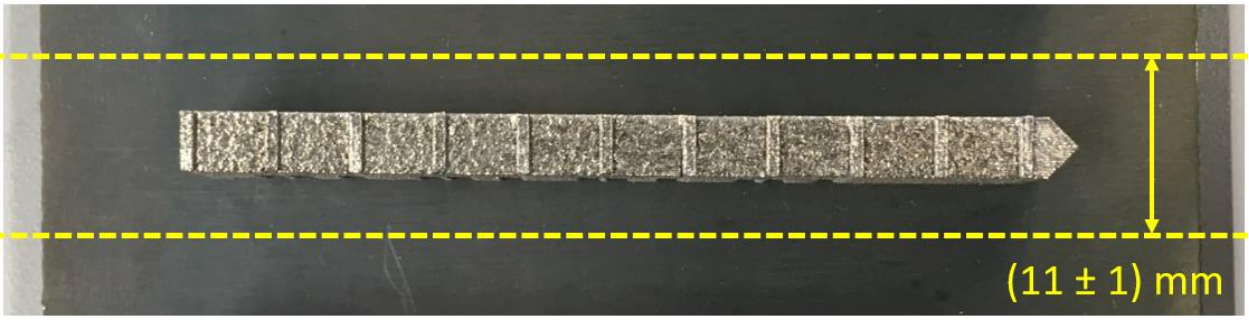

Figure 12: Individual parts are separated using two EDM cuts parallel to the part and 3 mm from each side.

2.6 Specimen Naming Convention

Any piece of material, from a complete build plate to an individual thin wall can be used as a measurement specimen or can be used to make a specimen. The following naming convention is used for almost all AMB2022-02 specimens:

AMB2022-718-AMMT-VR-PX-LY-WZ, with R = 6, 7, or 8,..., X = 1, 2, 3, 4; Y = 1,…, 12; Z = 1, 2, 3, 4

Here, "AMB2022" refers to the current round of AM Bench measurements, "718" refers to the alloy used, and "AMMT" refers to the build machine used to conduct the AM build. Note that in AMB2022-01, the build plates were given the designation B = Build plate, whereas for the variable scan strategy parts for AMB2022-02, these are designated V = variable scan plates.

Similar to other 2022 AM Bench designations, P = Part, L = Leg, W = Wall. The build plates (B or V) are numbered in the order they were built, and the bridge parts (P) and the thin walls (W) are numbered from the laminar flow side of the build plate with the sequence shown in the photograph in Figure 2b). The legs (L) are numbered as shown in Fig. 1. An example valid sample designation is

AMB2022-718-V7-P2-L10-W1.

This refers to variable scan plate 7, part 2, leg 10, and wall 1. Samples composed of multiple legs can be designated by listing them together:

AMB2022-718-AMMT-V7-P3-L1-L2-L3.

3. Measurement Descriptions

The AMB2022-02 benchmark measurements include in situ thermographic measurements during the build process, and ex-situ characterization of the part deflection. The measurement methods include:

In situ measurements during the build

- Use of in situ thermography to measure the location-dependent cooling rates of the solid material immediately after solidification (after the solidus is reached)
- Use of in situ thermography to determine the time above melting (above solidus/liquidus midpoint)

Ex situ measurements (scheduled, please see below)

- Distortion measurements comparing part geometry before and after partial cutting from the build plate

3.1 In Situ Time Above Melting

Methods for defining and extracting the location-specific 'time above melt' from thermographic data will largely follow those from prior AM-Bench challenges for 'melt pool length' (Heigel et al. 2020). The thermographic measurement setup and the data analyses used are the same as for the AMB2022-01 challenges. Modelers should refer to that document for more in-depth details. The following algorithm is repeated here to demonstrate calculation of 'time above melt' (t_{TaM}) for each pixel within the field of view of thermographic video data:

1) Convert thermal video to temperature utilizing assumed $\epsilon = 0.5$, resulting in temperature vs. time for each pixel (x_i,y_j) or $T(x_i,y_j,t)$.
2) Perform spatter removal algorithm and thresholding (to be detailed in later publications).
3) For each pixel (x_i,y_j):
    a. Extract temperature vs. time profile, $T(x_i,y_j, t)$
    b. Identify all timepoints where $T(x_i,y_j, t) = 1298$ °C (or the assumed mid-point between liquidus and solidus temperature), by finding the intersections.
    c. Identify the maximum time period, $\max(\Delta t_i)$ where $\mathbf{T(x_i,y_j, t) > 1298\ °C}$. Store as $t_{TaM}(x_i,y_j)$.
    d. If no $t_{TaM}(x_i,y_j)$ is identified, then store as 'not a number' $t_{TaM}(x_i,y_j)$ = NaN, or reject this pixel from further analysis.

Note that while the analysis of the thermographic data will utilize an assumed $T_{trans} = 1298$ °C, modelers using different thermodynamic material properties may wish to utilize a different temperature threshold that better represents the mid-point between liquidus and solidus of the IN718 material.

3.2 In Situ Cooling Rates

Similar to prior AM-Bench challenges (Heigel et al. 2020) and the 'time above melt' feature, surface cooling rates for the 3D builds with custom scan strategies will be calculated on a per-pixel basis as was done for the AMB2022-01 challenges. Additionally, similar temperature values and temperature range will be used to define 'cooling rate' as is used in AMB2022-03 challenges.

The cooling rate, $\Delta T/\Delta t$, will be based on linear interpolation of the temperature vs. time for each pixel, $T(x_i,y_j,t)$, during **the same temperature peak that 'time above melt' was calculated**. The ΔT is between the assumed solidus temperature $\mathbf{T_{solidus} = 1260\ °C}$, and 110 °C below, resulting in fixed $\mathbf{\Delta T = 110\ °C}$. Therefore, the objective then is to identify the time span $\mathbf{\Delta t = t_{1260} - t_{1150}}$, where t_{1260} is the timepoint where the temperature-time curve intersects T = 1260 °C, and t_{1150} where it intersects T = 1150 °C.

The following algorithm is used to extract solid cooling rate from the 3D build thermographic data:

1) Convert thermal video to temperature utilizing assumed $\epsilon = 0.5$, resulting in temperature vs. time for each pixel (x_i,y_j) or $T(x_i,y_j,t)$.
2) Perform spatter removal algorithm (to be detailed in later publications).
3) For each pixel (x_i,y_j):

a. Extract temperature vs. time profile, $T(x_i,y_j, t)$
b. Identify nominal time period when 'time above melt' is defined
c. Identify $\mathbf{t_{1260}}$, where $T(x_i,y_j, t)$ = 1260 °C (or the assumed solidus), by finding the intersection
d. Identify $\mathbf{t_{1150}}$, where $T(x_i,y_j, t)$ = 1150 °C, or 110 °C below the assumed solidus.
e. Calculate $\mathbf{\Delta t = t_{1260} - t_{1150}}$
f. Calculate SCR(x_i,y_j) = $\Delta T/\Delta t$ = (110 °C)/Δt, and store the value
g. If no SCR is identified, then store as 'not a number' SCR(x_i,y_j) = NaN, or reject this pixel from further analysis.

It is anticipated that modelers submitting results to CHAL-AMB2022-02-SCR will follow a similar algorithm and definition of SCR as described above. However, modelers are encouraged to test or implement any variation they determine as more appropriate (e.g., using a different solidus temperature), and discuss with fellow modelers and metrologists at the AM-Bench conference.

3.3 Part Distortion

Part distortion or deflection measurements for AMB2022-02 challenges will be the same as for the AMB2022-01 challenges. Please note that the Part Deflection measurement results for the CHAL-AMB2022-02-PD may not be available at the time model result submissions are due, so judging may be delayed. Modelers should periodically refer back to this document for updates.

After being built, the part remains on a section of the build plate. The tops of all 11 ridges are skim cut parallel to the build plate to remove the rough as-built surface to allow for more accurate measurement. The vertical height, relative to the surrounding base plate, of **every other ridge** on the stop surface of the part is measured using a coordinate measurement machine (CMM). **Six points** are sampled on the top of each ridge to ensure coverage of the surface. To minimize the influence of the build plate warp of the measurement, the areas adjacent to the ridges are used as the reference, as shown in the drawing below. Least-squares fit features will be utilized to evaluate the measurands. These initial measurements will make up $z_i^{initial}$, where $i = 1{:}\,6$ using the numbering in Figure 13 below.

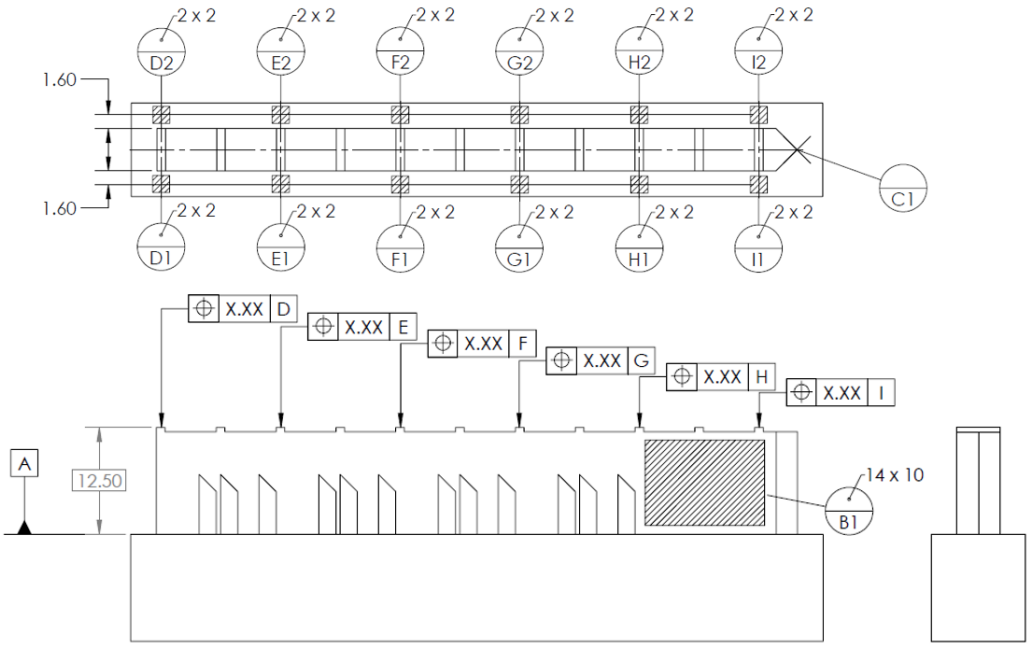

Figure 13: Measurement definition for part distortion measurements

Next, the part is EDM cut such that only the end portion of the part remains attached to the plate (see Figure 14), and the cut section of the part will deflect upward from relaxation of the as-built residual stresses. The part will then be measured again per the measurement definition using a CMM, and will make up z_i^{cut}.

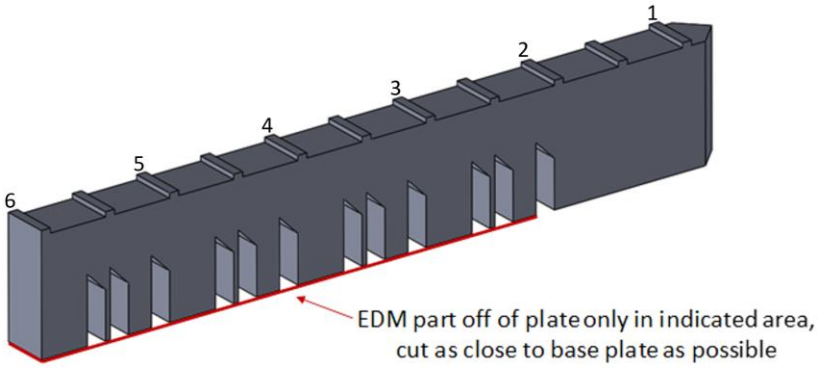

Figure 14: Ridge numbering and location of EDM cut which results in upward distortion

For these benchmark comparisons, the part distortion is defined by the vertical deflections of all measured ridge edges after being cut with EDM. Thus, $\delta_i = z_i^{cut} - z_i^{initial}$, where δ_i is the vertical deflection of edge *i*. The final qualitative result will be the vertical deflection of the component estimated at the center of the measurement ridge for each of the six ridges. An uncertainty value for the measured deflection will be provided and will be calculated based on substitution measurements.

4. Description of Benchmark Challenge Problems

4.1 In Situ Build Benchmarks

4.1.1 CHAL-AMB2022-02-TAM

The 'time above melt' modelling challenge will be based on eight individual selected layers from each of the three 3D builds with custom scan strategies listed in Table 2. The eight layers span the general range of geometric features and laser scan directions. Figure 15 gives an outline of the eight layers that will be used in the challenge, and Table 5 provides more detail.

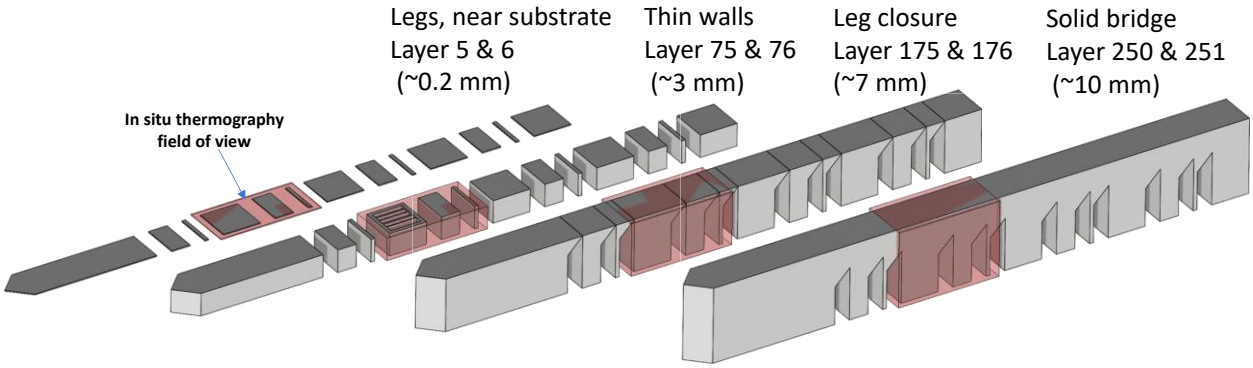

Figure 15: The eight selected layers for the CHAL-AMB2022-02-TAM and CHAL-AMB2022-02-SCR modelling challenges, and the relative position with respect to geometric features on the bridge structure.

Table 5: The eight layers to be modelled in the CHAL-AMB2022-02-TAM and CHAL-AMB2022-02-SCR modelling challenges. Each of the eight layers should be modelled for each of the three custom scan strategy builds listed in Table 2.

Challenge Layers	Approx. Layer Height (mm)	Part Features	Laser Scan Orientation
5	0.2	Legs, near substrate	Vertical
6	0.24	Legs, near substrate	Horizontal
75	3	Legs and thin walls	Vertical (thin walls horizontal)
76	3.04	Legs and thin walls	Horizontal
175	7	Leg closure	Vertical
176	7.04	Leg closure	Horizontal
250	10	Solid bridge	Horizontal
251	10.04	Solid bridge	Vertical

Modelers are to calculate 'time above melting' as close as possible to the definition or algorithm described in Section 3.1. After extracting 'time above melting' values, modelers should select TaM values from a region that is nominally commensurate with the in situ thermal camera field of view covering legs 8, 9 and 10. From these extracted TaM values, for each of the 8 layers, and each of the three custom scan-strategy builds, modelers should calculate the following statistical features for the CHAL-AMB2022-02-TAM modelling challenge:

- Number of pixel/element/nodes that TaM is interrogated from model results (e.g., sample size)
- Mean of all pixel/element/nodal TaM values
- Median of all pixel/element/nodal TaM values
- Standard deviation of all pixel/element/nodal TaM values

The AMB2022-02 challenge description dataset provides three submission templates to be provided by modelers for submission to the CHAL-AMB2022-02-TAM challenge. All three should be submitted as part of the challenge:

- CHAL-AMB2022-02-V6-TAM submission template.csv
- CHAL-AMB2022-02-V7-TAM submission template.csv
- CHAL-AMB2022-02-V8-TAM submission template.csv

Additionally, modelers should supply pictures and/or a brief description of the model formulation and visualization of results as described above for the CHAL-AMB2022-02-TAM challenge, and consider providing tabulated TAM results data to AM-Bench organizers, although this will not be considered as part of the challenge judging.

4.1.2 CHAL-AMB2022-01-SCR

Modelers are to calculate the 'solid cooling rate' (SCR), as close as possible to the definition or algorithm described in Section 3.2, for the same layers to be modelled for the 'time above melt' challenge described in Table 5. After extracting SCR values, modelers should select values from a region that is nominally commensurate with the in situ thermal camera field of view. From these extracted SCR values, and for each of the 8 layers, modelers should calculate the following statistical features for the CHAL-AMB2022-01-SCR modelling challenge:

- Number of pixel/element/nodes that SCR is interrogated from model results (e.g., sample size)
- Mean of all pixel/element/nodal SCR values
- Median of all pixel/element/nodal SCR values
- Standard deviation of all pixel/element/nodal SCR values

The AMB2022-02 challenge description dataset provides three submission templates to be provided by modelers for submission to the CHAL-AMB2022-02-TAM challenge. All three should be submitted as part of the challenge:

- CHAL-AMB2022-02-V6-SCR submission template.csv
- CHAL-AMB2022-02-V7-SCR submission template.csv
- CHAL-AMB2022-02-V8-SCR submission template.csv

Additionally, modelers should supply pictures and/or a brief description of the model formulation and visualization of results as described above for the CHAL-AMB2022-02-SCR challenge, and consider providing tabulated SCR results data to AM-Bench organizers, although this will not be considered as part of the challenge judging.

4.1.3 CHAL-AMB2022-01-PD

The δ_i will be measured for the six ridges investigated and modelers should attempt to extract similar information from their models by estimating the deflection for each ridge perpendicular to each feature's respective datum at the center of the measurement ridge. Modelers should provide a δ_i for each of the of the six ridges described rounded to three significant digits (e.g. X.XXX mm), and for each of the three custom scan strategy 3D builds listed in Table 2. Modelers will be judged by calculating the RMS error between the modeled and measured deflection values using a weighted constant, α_i, which gives higher weight to the struts on a longer portion of unsupported material (i.e., the point of greatest anticipated deflection). This metric and the values for α_i are given below.

$$\Delta = \sqrt{\sum_{i=1}^{6} \left(\alpha_i * (\delta_i - \delta_{i,model})\right)^2}$$

i	1	2	3	4	5	6
α_i	1	1	2	3	4	5

Please note that the Part Deflection measurement results for the CHAL-AMB2022-02-PD may not be available at the time model result submissions are due, and judging of this challenge problem may be delayed. Modelers should periodically refer back to this document for updates.

5. Description and Links to Associated Data

All data available to support the AMB2022-02 challenges are contained in the "AM Bench 2022 3D Build with Custom Laser Scan Strategies Modeling Challenge (AMB2022-02)" dataset available here: https://doi.org/10.18434/mds2-2617.

New data files, updates, and/or changes to download URLs may be made periodically. Users should refer to the README text file which will record all updates. Additionally, the NIST Public Data Repository (PDR) undergoes frequent updates. If file downloads fail or are unavailable, users should wait several hours before contacting the technical support listed on the AMB2022-02 dataset webpage.

6. References

Citations are provided throughout this document as hyperlinked URLs to the associated digital object identifier (DOI). Clicking these hyperlinked text should open the associated publication or cited source.

†Disclaimer

The National Institute of Standards and Technology (NIST) uses its best efforts to deliver high-quality copies of the AM Bench database and to verify that the data contained therein have been selected on the basis of sound scientific judgment. However, NIST makes no warranties to that effect, and NIST shall not be liable for any damage that may result from errors or omissions in the AM Bench databases.

Certain commercial equipment, instruments, or materials are identified in this paper in order to specify the experimental procedure adequately. Such identification is not intended to imply recommendation or endorsement by NIST, nor is it intended to imply that the materials or equipment identified are necessarily the best available for the purpose.